IJST, Transactions of Civil and Environmental Engineering, Vol. 35, No. C1, pp 35-50
Printed in The Islamic Republic of Iran, 2011

NUMERICAL INVESTIGATION ON THE BEHAVIOR OF FRP-RETROFITTED RC EXTERIOR BEAM-COLUMN JOINTS UNDER CYCLIC LOADS*

A. DALALBASHI ESFAHANI[1], D. MOSTOFINEJAD[1,**], S. MAHINI[2] AND H. R. RONAGH[3]

[1]Dept. of Civil Engineering, Isfahan University of Technology (IUT), Isfahan, I. R. of Iran
Email: dmostofi@cc.iut.ac.ir
[2]Dept. of Civil Engineering, Yazd University, Yazd, I. R. of Iran
[3]Division of Civil Engineering, School of Engineering, the University of Queensland, Brisbane, Australia

Abstract– This paper reports on the capability of nonlinear quasi-static finite element modeling in simulating the hysteretic behavior of FRP-retrofitted reinforced concrete (RC) exterior beam-column joints under cyclic loads. For the purposes of our investigation, three concrete beam-to-column joint specimens (un-strengthened and FRP-strengthened) were selected. The ANSYS finite element software was used for modeling RC exterior joints. The specimens were loaded using a step-by- step load increment procedure to simulate the cyclic loading regime employed in testing. Additionally, an automatically reforming stiffness matrix strategy was used to simulate the actual seismic performance of the RC members after cracking, steel yielding, and concrete crushing during the push and pull loading cycles. The results show that the hysteretic simulation is satisfactory for both un-strengthened and FRP-strengthened specimens. Furthermore, when FRP strengthening is employed, strengthened beam-column joints exhibit a better structural performance than the un-strengthened specimens.

Keywords– Beam- column joint, cyclic load, finite element method, FRP sheets, hysteretic curve, reinforced concrete, strengthening

1. INTRODUCTION

Many reinforced concrete (RC) frame buildings located in seismic zones are deficient to withstand moderate to severe earthquakes [1]. Hysteretic behavior of structures subjected to cyclic loads can be explained by the behavior of structures under earthquake load. For example, if the hysteretic curve has a narrow and low strength loop, it will be accompanied by limited energy dissipation and ductility, while the wide loop and high strength hysteretic curve represents more ductility and energy dissipation [1].

Over the past half century, many researchers have tried to understand the behavior of buildings under lateral loads in order to design earthquake-resistant structures. In the Second World Conference on Earthquake Engineering (Tokyo & Kyoto, 1960), many research papers were presented on the elasto-plastic response of simple structural systems using the then-developing computers, placing more emphasis on the development of numerical procedures for nonlinear dynamic response analysis [2]. The effect of some hysteretic characteristics on the response of single-degree-of-freedom systems, also the effects of different hysteretic parameters on the earthquake response analysis were discussed by Otani [3]. Modeling the complex behavior of reinforced concrete, which is both non-homogeneous and anisotropic, has been a difficult challenge in the finite element analysis of civil engineering structures. Most early finite element models of reinforced concrete included the effects of cracking based on a pre-defined crack pattern [4, 5].

*Received by the editors July 25, 2009; Accepted June 16, 2010.
**Corresponding author

In recent years, more studies and tests have been conducted on beam-column joints due to their important role in structural stability. Designing beam-column joints is considered to be a complex and challenging task for structural engineers. Careful design of joints in RC frame structures is crucial to structural safety. Many methods have been proposed to increase joint strength. For instance, a number of studies have used externally bonded FRP composites in order to increase shear, flexural, and anchorage capacity of RC frame joints. Mahini et al. [6] proposed a practical technique for flexural repair of exterior beam-column joints using CFRP wraps. They tested RC beam-column joints before and after repair under a monotonic load and checked their results against a non-linear finite element analysis using ANSYS. The results indicated that ANSYS could be used as a tool for understanding the behavior of RC beam-column joints.

Mostofinejad & Talaeitaba [7] proposed a finite element (FE) model for the non-linear analysis of RC joints covered with FRP overlays. The results showed that good ductility and strength enhancement were achieved by employing appropriate FRP laminates. Parvin & Wu conducted a numerical analysis to investigate the effect of ply angle on the improvement of shear capacity and ductility of beam-column joints strengthened with CFRP wraps under combined axial and cyclic loads [8]. Their finite element analysis entailed profiling the behavior of three beam-column joints strengthened with CFRP wrapping with various ply angle configurations. Parvin & Wu (2007) [8] found that four layers of wrapping placed successively at ±45° ply angles with respect to the horizontal axis formed the most suitable upgrade scheme for improving shear capacity and ductility of beam-column connections under combined axial and cyclic loads.

Xue et al. [9] tested seven high-performance concrete (HPC) beams and two counterpart normal-strength concrete (NC) beams under reversed cyclic vertical displacement to investigate the seismic behaviors of normal and pre-stressed HPC beams. The failure patterns, skeleton curves, hysteretic model, displacement restoring capacity, ductility, stiffness degradation and energy dissipation capacity of HPC beams are discussed. Vasdravellis et al. [10] carried out experimental tests and numerical analyses to study the seismic behavior of semi rigid partial-strength steel–concrete composite beam-to-column joints. They tested four full-size sub-assemblages representing exterior composite beam-to-column joints under cyclic loading. They investigated the hysteretic behavior and the dominant failure modes of the tested sub-assemblages, the contribution of the column web panel to the overall joint rotations and the mechanisms which may describe the force transfer between the concrete slab and column, and also finite element models of the tested specimens were developed and numerical analyses were carried out in order to further investigate the stress state in the composite sub-assemblages and to study the influence of various parameters on the joint behavior [10]. A comprehensive experimental study was also carried out on the exterior RC joints strengthened with FRP under simulated seismic load by Antonopoulos and Triantafillou [11].

In this paper, to calibrate and verify the nonlinear FE modeling, first the exterior beam-column connection (un-strengthened and strengthened with CFRP) tested by Mahini et al. [12] will be modeled using ANSYS software; and the hysteretic curves and failure mode of this connection will be extracted and compared with the experimental results. Then, the hysteretic curves, failure mode, and the proposed hysteretic model of some other RC joints will be evaluated.

2. HYSTERETIC BEHAVIOR OF REINFORCED CONCRETE MEMBERS

A typical lateral load-displacement hysteretic curve for a reinforced concrete member is shown in Fig. 1, in which the curve is obtained through the slender column test [13]. The loading in cycles 1 and 2 was up

to onset of yielding of the reinforcement, while loading in cycles 3 and 4 included the post yield resistance of the column. The last loading cycle showed strength degradation.

The general hysteretic characteristics can be summarized as follows [2]:

(a) Stiffness changes due to the flexural cracking of concrete and the tensile yielding of the longitudinal reinforcement (cycle 1);

(b) When a deflection reversal is repeated at the same newly attained maximum amplitude, the loading stiffness in the second cycle is noticeably lower than the one in the first cycle, although the resistances at the displacement peak are almost identical (cycles 3 and 4). This reduction in stiffness could be attributed to the formation of cracks during loading cycle 3, and also to a reduced stiffness of the longitudinal reinforcement in cycle 4 due to the Bauschinger effect. The yielding of the longitudinal reinforcement is also observed in cycle 3.

(c) Average peak-to-peak stiffness of a complete cycle decreases with the preceding maximum displacement. Note that the peak-to-peak stiffness of cycle 5 is significantly smaller than that of cycle 2, although the displacement amplitudes of the two cycles are comparable. The peak-to-peak stiffness of cycle 5 is closer to that of cycles 3 and 4.

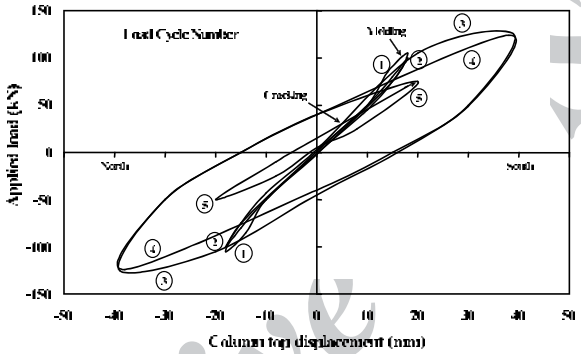

Fig. 1 Hysteretic behavior of a reinforced concrete column [2]

A hysteretic model for the reinforced concrete must be able to describe the above-mentioned characteristics. The observation is limited to the dominantly flexural behavior of the reinforced concrete member. Also, it must be able to provide the stiffness and resistance under any displacement history. Some hysteretic models are supposed, and include many hysteretic rules. Different hysteretic models representing the dominantly flexural behavior of reinforced concrete are briefly described in this section. The following definitions are used to simplify the description of the hysteretic conditions [2]:

Loading: The amplitude (positive or negative) of resistance increases without change in sign;

Unloading: The amplitude (positive or negative) of resistance decreases without change in sign;

Load reversal: The sign of resistance changes and the response point crosses the displacement axis;

Primary curve: A resistance-displacement relation curve under monotonically increasing load;

Unloading point: A resistance-displacement point from which unloading has started.

3. FINITE ELEMENT MODELING

A three-dimensional nonlinear finite element model for the beam-column connection is developed using ANSYS. To model the characteristics of concrete, an eight-node solid element, Solid 65, is used [14]. The solid element has eight nodes with three degrees of freedom at each node–translation in the nodal x, y, and z directions. The element is capable of plastic deformation, simulating the cracking and crushing of concrete. The William-Varnk criterion is used for fracture modeling in concrete. This model is capable of accounting for the cracking of concrete in tension and crushing of concrete in compression. Some

important parameters to perform the failure envelope in the model are elastic modulus (E_c), ultimate uniaxial compressive strength (f'_c), ultimate uniaxial tensile strength (modulus of rupture, f_r), Poisson ratio (v), and the shear transfer coefficients for open and closed cracks. Also, the Hognestad's model is used for modeling the compressive strength of concrete. In addition, to model the longitudinal reinforcement and the FRP composites, Link 8 and Solid 45 elements are used, respectively. In order to model the FRP composites, an anisotropic material called ANISO is employed. A bi-linear stress-strain curve is used to model the material in both compression and tension and in any direction of x, y, and z. A multi-linear isotropic stress-strain curve is also considered for the stress-strain curve.

4. VALIDAION OF FINITE ELEMENT MODEL

In this part, two RC beam-column connections before and after FRP reinforcement tested by Mahini et al (CSC1 & RSC1) [12] under cyclic loads are numerically evaluated as shown in Fig. 2. Then, the numerical and experimental results are compared to show the reliability and validity of the results.

No debonding was observed during the experiments and perfect bond between materials and concrete was, therefore, considered such that adjacent elements had common nodes. In Fig. 3, a typical finite element model is shown. Cyclic loads are applied with a step-by-step strategy in a displacement control regime similar to the tests shown in Fig. 4. Each cycle is modeled in a load step and each load step is divided into a number of sub-steps. At the initial step of the analysis, because the section is un-cracked and the solution is linear, a lower number of sub-steps are taken into consideration. However, at the cracking load and the final cycles, more load steps and sub-steps are utilized. An automatically reforming stiffness matrix is employed in order to simulate the cracking and crushing of concrete and yielding of steel during cyclic loading.

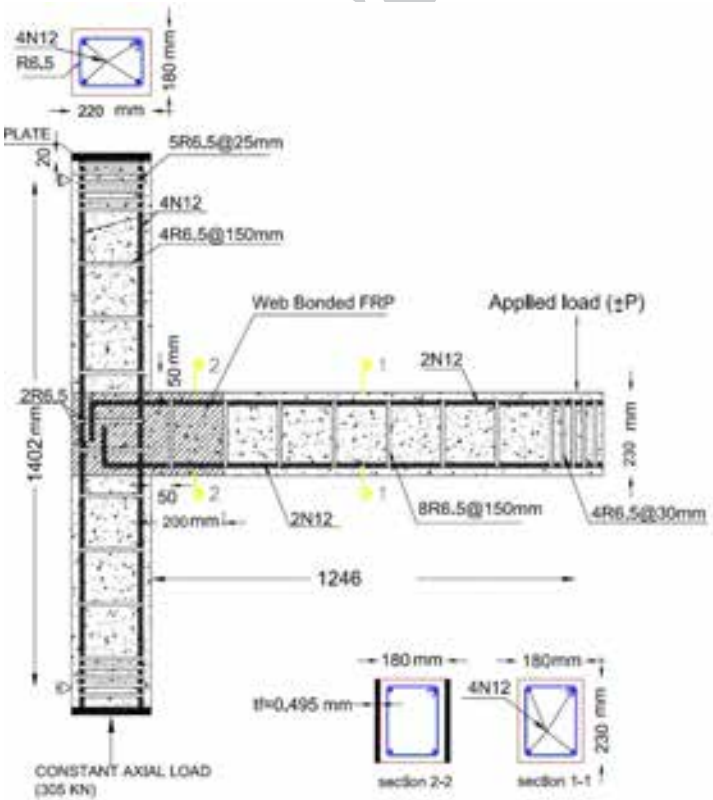

Fig. 2. Specimen detail: plain CSC1 and FRP-retrofitted RSC1 [12]

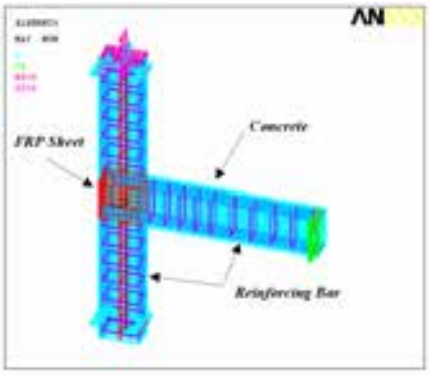

Fig. 3. Specimen analytical details

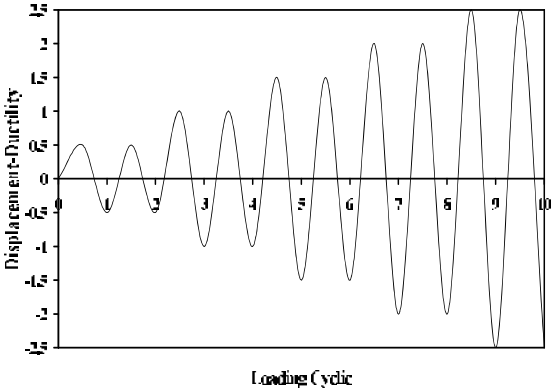

Fig. 4. Analytical loading regime

a) Experimental model

CSC1 & RSC1 specimens represent a scaled down exterior connection of a typical RC residential building design according to AS 3600 (2001) [15]. The connection consists of a beam 180 mm wide and 230 mm deep and a column of 220 mm×180 mm. The beam is reinforced with high-strength longitudinal reinforcing steel bars 12 mm in diameter with two bars at the top and two at the bottom of the beam. The column is reinforced with four N12 (12 mm in diameter) reinforcing bars, with one bar positioned in each corner of the column. The beam stirrups and column ties are 6.5 mm bars at 150 mm centers. Ties are also placed in the connection region in accordance with the earthquake loading requirements of AS 3600 (2001). The proposed retrofitting system consists of three plies of web-bonded CFRP sheets. All layers are unidirectional sheets and are applied over a length of 200 mm from the column face on the beam-end with fiber directions parallel to the longitudinal beam axis as shown in Fig. 2. Concrete compressive strength, elastic modulus, and splitting strength (Table 1) of the CSC1 & RSC1 specimens were determined on the day of testing each connection. Yield strength of N12 reinforcing steel bars and R6.5 mm stirrups and ties were also tested as being 500 MPa and 380 MPa, respectively. The carbon fibers used had a thickness of 0.165 mm with a maximum elongation of 1.55% and a tensile strength of 3900 MPa according to the manufacturer's specifications [12].

Table 1. Mechanical properties of concrete [12]

Specimen	Compressive strength (MPa)	Modulus of elasticity (GPa)	Tensile strength (MPa)
CSC1	40.73	30.17	3.29
RSC1	36.44	29.7	3.62

b) Results of specimen CSC1

According to the experimental study reported by Mahini et al [12], the plain specimen was loaded in two phases. The first phase included cycles that cause cracking and the second phase included cycles that cause yielding of the longitudinal reinforcement followed by failure of the joint. In the analytical modeling, this specimen was loaded in a similar manner. As shown in Fig. 5, a plastic hinge was formed at the face of the column in finite element analysis, similar to the experimental observation (Fig. 6). Also, investigation of the strain variation along the longitudinal reinforcement showed that maximum strain happens at the face of the column (Fig. 7). In Fig. 8, the hysteretic curves of the specimen obtained from experimental and analytical studies are compared. It is observed in the figure that the experimental and numerical hysteretic curves are reasonably similar. The difference between the two can even become less distinguishable if a finer mesh is used in the numerical simulation.

Examination of the hysteretic curves reveals that yield stress in the analytical solution is achieved at a displacement of 15.8 mm, where maximum displacement and load are approximately 23.3 mm and 19.42 kN, respectively. In the experimental results, the displacement at yield and maximum displacement are equal to 15.8 and 26.6 mm, respectively, with a maximum load of 19.51 kN. The envelopes of the beam tip load-displacement curves of both the experimental and numerical specimens are compared in Fig. 9. The graph shows that both experimental and numerical specimens have a similar trend in the positive area. However, in the negative region, up to 20 percent difference is observed in experimental and numerical results, which contributes to the size of meshing and intrinsic complexity of nonlinear modeling of hysteresis behavior.

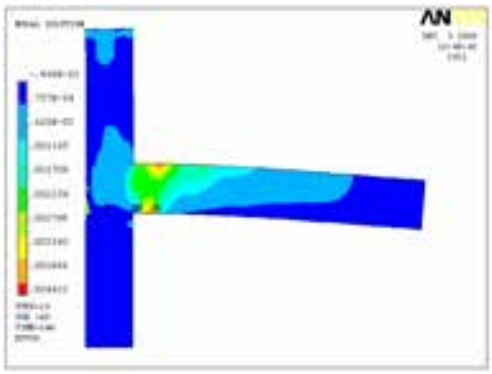

Fig. 5. Failure mechanism of CSC1 obtained from numerical modeling

Fig. 6. Observed failure mechanism of specimen CSC1 [12]

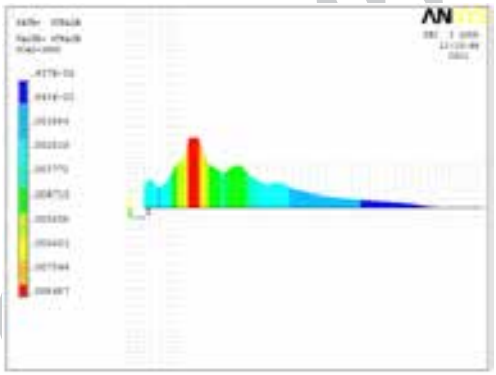

Fig. 7. Strain variation in the CSC1 longitudinal reinforcement obtained from numerical modeling

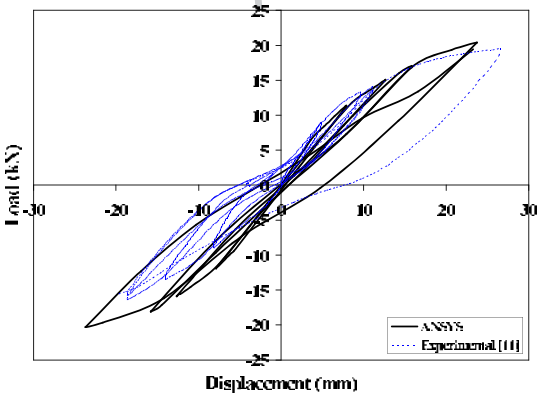

Fig. 8. Comparison of hysteretic curves obtained for plain specimen CSC1

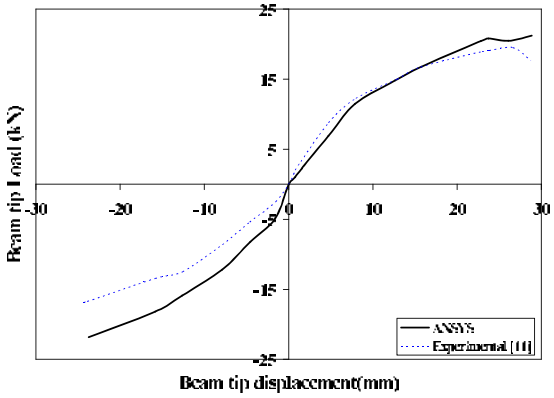

Fig. 9. Load versus displacement for specimen CSC1

c) Results obtained for RSC1 retrofitted specimen

RSC1 specimen was subjected to the same loading regime as specimen CSC1. Fig. 10 shows the final failure of the specimen at which the plastic hinge formed beyond the cut–off point of the CFRP. In fact, CFRP reinforcement causes the plastic hinge to move from the face of the column toward the beam. This can also be seen in the experimental observations (Fig. 11). CFRP effect on moving the plastic hinge can be better observed with comparison of the strain variation along the longitudinal reinforcement in both specimens (Figs. 7 and 12). Comparison of the hysteretic curves obtained from both the analytical and experimental specimens in Fig. 13 shows that energy absorption persists as the maximum load is maintained to the end. The curves depict that the first yield load of the analytical curve is equal to that of the experiment (16 kN) and so it is the maximum load (23.67 kN) as shown in Fig. 13. The envelopes of the beam tip load-displacement curves of experimental and numerical specimens are depicted in Fig. 14. The curve illustrates a similar trend for both experimental and numerical specimens, especially in the positive region; although in the negative area there are some discrepancies in the results. Fig. 15 illustrates the stress variation along the CFRP sheets of the numerical retrofitted specimen. Maximum stress occurred in the middle of the CFRP sheets, which is 140 N/mm^2 in the face of the column.

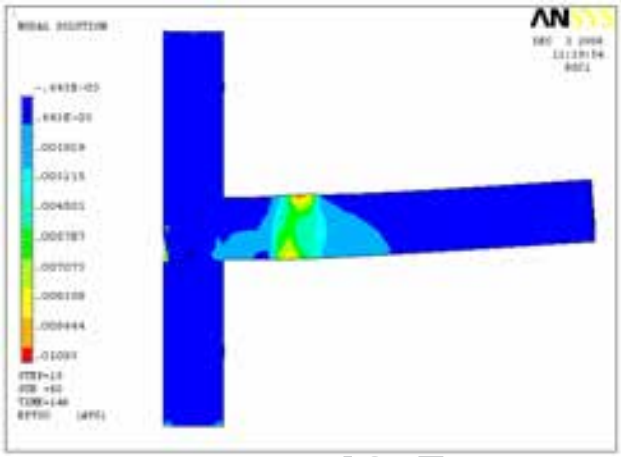

Fig. 10. Failure mechanism of RSC1 obtained from numerical modeling

Fig. 11. Observed failure mechanism of specimen RSC1 [12]

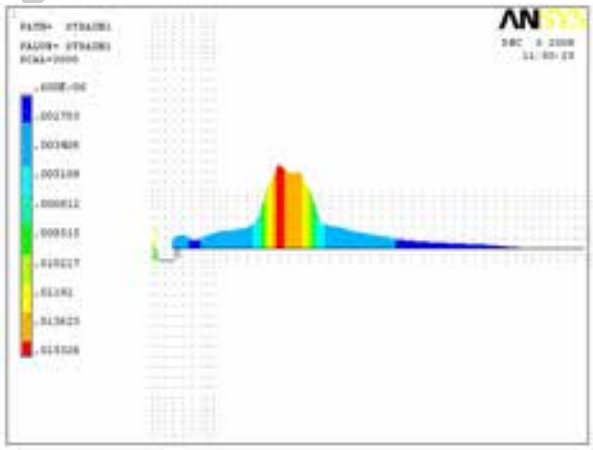

Fig. 12. Strain variation along the longitudinal reinforcement of specimen RSC1 obtained from numerical modeling

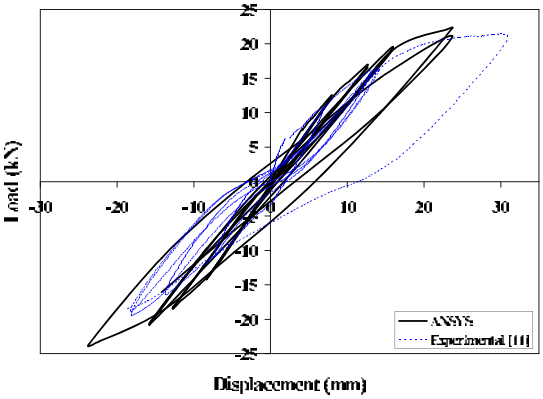

Fig. 13. Comparison of hysteretic curves obtained for specimen RSC1

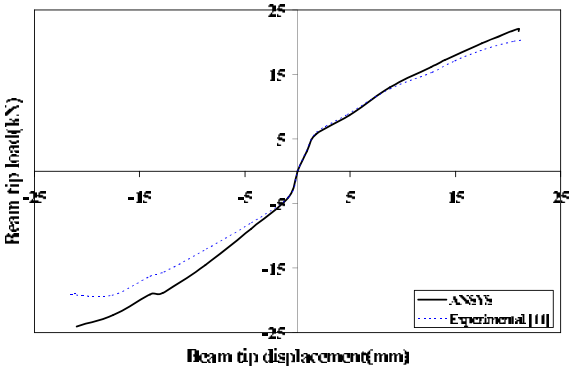

Fig. 14. Load versus displacement for specimen RSC1

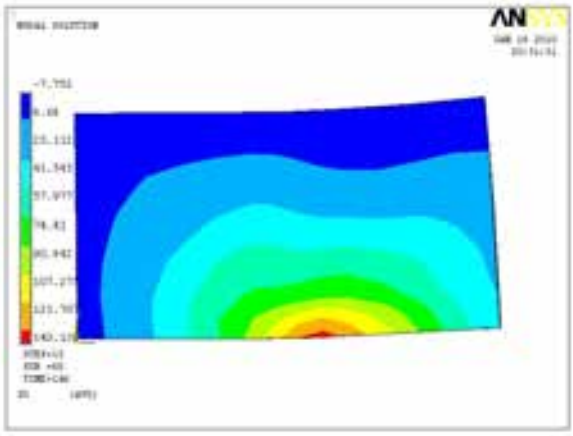

Fig. 15. Strain variation along the CFRP sheets for specimen RSC1 obtained from numerical modeling

d) Behavior of hysteretic curves

The hysteretic curve loop of the RSC1 specimen obtained from experimental work as well as finite element modeling is shown in Fig. 16. Both curves show similar behavior, i.e. punching in the middle and stiffness degrading after cracking of concrete. As it is seen in Fig.16, OA is a straight line, which describes the linear elastic behavior of reinforced concrete. Notice that the cracking and stiffness degrading curve moves toward B, which is the unloading point. Beyond this point, the displacement axis is cut by a straight line graph at point C, which starts the reverse loading. An explanation similar to that on the loading process can be provided for the reverse loading region and the next unloading, except that the response point in the following cycle moves to the maximum displacement point in the preceding cycle (B).

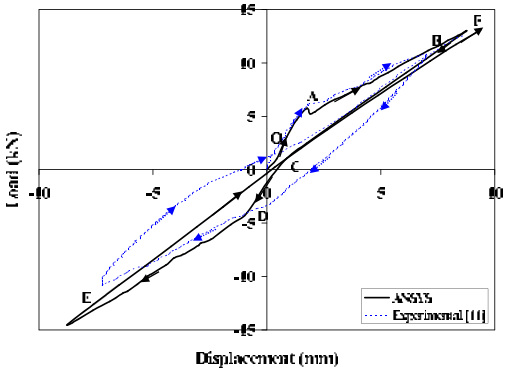

Fig. 16. Behavior of hysteretic curve (Specimen RSC1)

5. THE BEHAVIOR OF FULL-SCALE RC JOINTS

In this part, two exterior RC beam-column joints are selected. The first one is the joint with the shear failure (FM1) tested under cyclic load by Ghobarah and Said [16]. Ghobarah and Said then reinforced the joint core with GFRP sheets (FM1-R), and retested it. The second joint is selected from a frame of a typical RC residential building designed by ACI 318 [17] (FM2).

a) Joints description

FM1 specimen is the exterior beam-column joint whose detail is a lot like the buildings designed before the 1970's. Specimens FM1 and FM1-R represent a full scale connection. No transverse reinforcement was initially installed in the beam-column joint. The top and bottom longitudinal reinforcements of the beam were four M20 bars each, as shown in Fig. 17. The transverse reinforcement of the beam was M10 rectangular ties starting 75 mm from the face of the column. The ties were spaced at 150 mm for 600 mm and then spaced at 200 mm for 1000 mm, ending at 75 mm from the free end of the beam. The beam-column joint was expected to fall by joint shear before a plastic hinge is formed in the beam due to the lack of transverse reinforcement in the joint. The beam-column joint specimen designated as FM1 was tested as a control specimen. The joint core was repaired and rehabilitated using one layer of GFRP sheet. The height of the column and the length of the beam represent the distance to the contra-flexure points in the frame. The column was 3000 mm high with cross section dimensions of 250 × 400 mm (gross cross sectional area A_g =100,000 mm^2). The beam length was 1750 mm from the face of the column to the free end with a cross section of 250 × 400 mm. The longitudinal reinforcement used in the column was 6 M20 bars (equivalent to 19.5 mm diameter bar), in addition to two M15 bars (equivalent to 16.0 mm diameter bar) without splicing. The transverse reinforcement in the column was M10 rectangular ties with a single M10 supplementary central leg. The ties started 80 mm above and below the beam and were spaced at 200 mm as shown in Fig. 17. The concrete had a compressive strength equal to 30.8 MPa and the reinforcing steel had a yield stress of 454 and 425 MPa for the M10 and M20 bars, respectively. Following the practice before the seismic design codes were available, U–shaped GFRP laminates were installed and then the test was conducted. The repaired and rehabilitated specimen was designated FM1-R. Also, the loading regime for FM1 and FM1-R specimens is similar to that of the experimental specimen, as shown in Fig. 4 [12].

FM2 and FM2-R specimens are exterior joints which are 500 mm wide and 500 mm deep for both the beam and the column. All beams are reinforced with high-strength longitudinal reinforcing steel bars of Φ30 at the top and Φ25 at the bottom of the beam. All columns are reinforced with sixteen Φ20 reinforcing bars, five on each side of the column. The beam stirrups and column ties are 10 mm bars at 225 mm centers. Ties are also placed in the connection region in accordance with the earthquake loading requirements of ACI 318 [17]. For moving the plastic hinge from the face of the column toward the beam, a retrofitting system consisting of three plies of web-bonded CFRP sheets is proposed. All layers are unidirectional sheets and are applied over a length of 500 mm from the column face on the beam-end with fiber directions parallel to the longitudinal beam axis (Fig. 18). Fig. 4 shows the loading pattern for the FM2 and FM2-R specimens. This curve can be obtained through two methods. In the experimental test, bar yield displacement and maximum displacement are obtained. Then, displacement ductility is obtained by dividing maximum displacement to yield displacement. The concrete compressive strength is 27.5 MPa and the reinforcing steel has a yield stress of 412 MPa. Finally, the loading cyclic regime is propagated from displacement ductility and loading cyclic. However, because specimen FM2 was not an experimental test, maximum and yield displacements are obtained by ANSYS software.

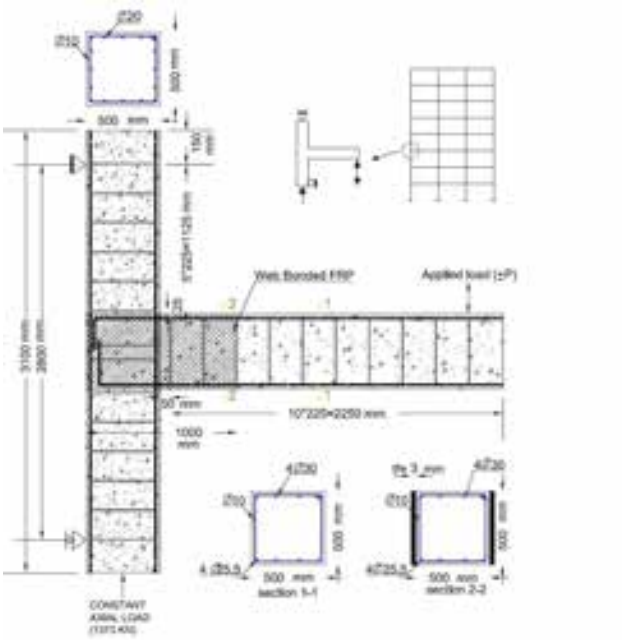

Fig. 17. Specimen detail: plain FM1 and GFRP-retrofitted FM1-R [16]

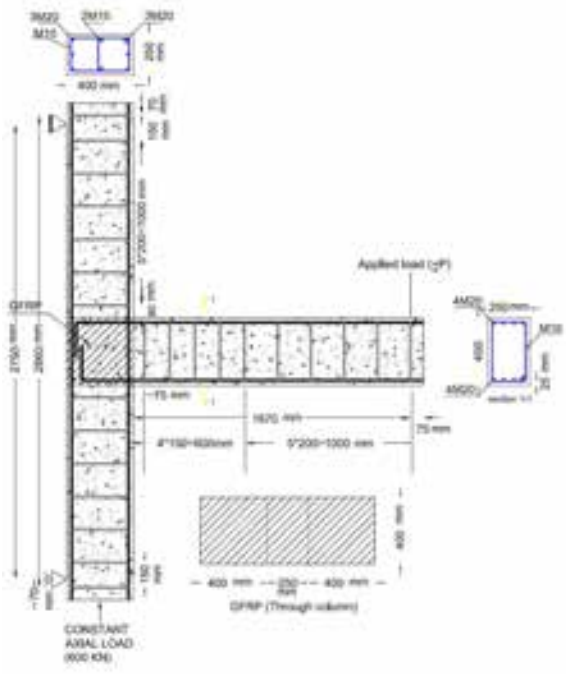

Fig. 18. Specimen detail: plain FM2 and GFRP-retrofitted FM2-R

b) Results of FE modeling for specimen FM1

In the experimental study reported by Ghobarah et al., specimen FM1 was tested under a reversed cyclic load applied at the beam tip. Before the first yield of longitudinal beam reinforcement, a diagonal shear crack was noted in the joint area in each loading direction forming an X-pattern. In the analytical modeling, whose loading is similar to that of the test specimen, the first crack is observed at the column face. The cracking load in the experimental specimen was 22 kN, so that its value equals 24 kN for the numerical specimen. Also, at failure, shear cracks are diagonal in the connection core (Fig. 19). The concrete strain alteration value is depicted in Fig. 20 in which the concrete strain is about 0.002 as far as failure occurs at this connection. Failure strain expands in the joint core and at the face of the column. This pattern shows that the failure mode is a shear one.

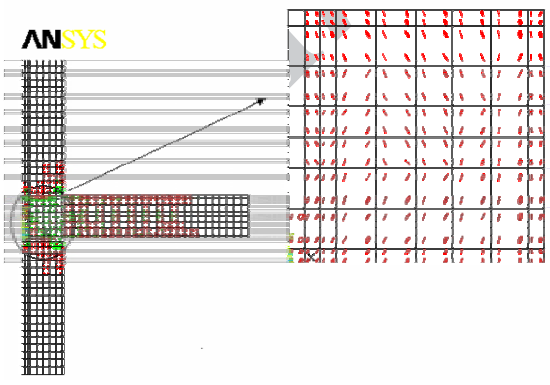

Fig. 19. Joint shear failure of specimen FM1 obtained from numerical modeling

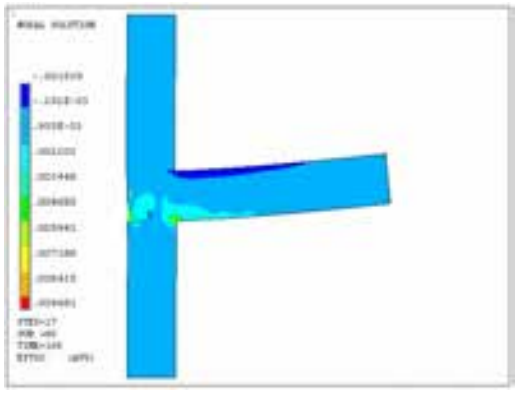

Fig. 20. Joint shear failure of specimen FM1 obtained from numerical modeling

A hysteretic curve of the specimen obtained from the analytical study is shown in Fig. 21. The envelopes of the beam tip load-displacement curves of the experimental and numerical specimens are illustrated in Fig. 22. The curve shows a similar trend in both positive and negative regions with some small

discrepancies. Table 2 presents the comparative results of the experiment by Ghobarah et al. [9] and the numerical analysis results obtained from the Finite Element Model (FEM) performed in this study. The finite element analysis and experimental results are in good agreement with less than 10% difference, which would have possibly decreased if a finer mesh had been used in the simulation. Nevertheless, the FEM model developed here is assumed to be adequate for the purposes of this study.

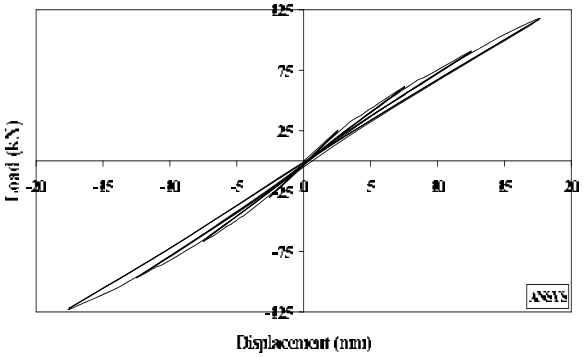

Fig. 21. Hysteretic curve for specimen FM1

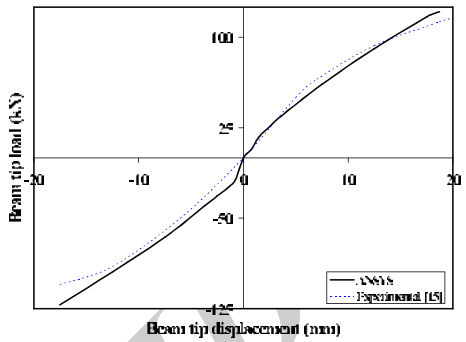

Fig. 22. Load versus displacement of specimen FM1 for numerical & experimental specimens

Table 2. Comparison of experimental and FE results (FM1)

FM1 Specimen	Cracking load (kN)	Failure load (kN)
Experimental	22	116.08
Numerical	24	110.22
Discrepancy	9.10%	5.10%

c) Results of FE modeling for specimen FM1-R

Plain exterior joint (FM1) is reinforced by bi-directional GFRP sheets (along the 45° direction) modeled by solid 45 element in ANSYS shown in Fig. 23. The 1.1 mm thick composite material has tensile strength of 552 MPa, elastic modulus of 27.6 GPa, and ultimate elongation of 1.7%.

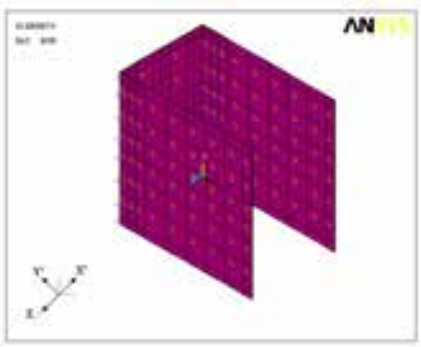

Fig. 23. Modeling of bi-directional GFRP using solid 45 element

The numerical specimen FM1-R uses the same loading regime as that of specimen FM1. In Fig. 24, the hysteretic curve of the specimen obtained from the analytical study is depicted. Comparison of both hysteretic curves obtained from analytical and experimental specimens indicates that the up-load and down-load in the experimental specimen are 126.23 and -114.61 kN, respectively, but those in the analytical hysteretic curve are 118 and -122 kN. The envelopes of the beam tip load-displacement curves of the experimental and numerical specimens are shown in Fig. 25. The graph shows that both experimental and numerical specimens have a similar trend. However, about 10 percent difference in the maximum load is observed in the negative region.

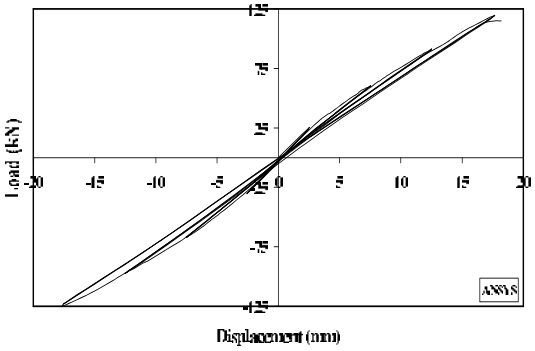

Fig. 24. Hysteretic curves for specimen MF1-R

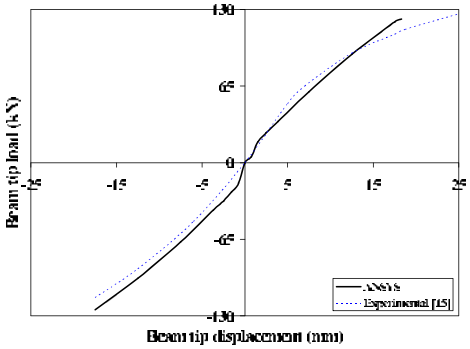

Fig. 25. Load versus displacement of specimen FM1-R for numerical & experimental specimens

The use of a GFRP plate in the joint has brought about the recovery behavior of the connection, as shown in Fig. 26, such that strain alteration in the joint is less than ε_c (ε_c= 0.002). As a result, the plastic hinge is formed at the face of the column, and has caused the joint to have a flexural mode of failure. The stress variations along the CFRP sheets of numerical retrofitted specimen are shown in Fig. 27. Maximum stress is 80 N/mm^2 in the joint region close to the column face. However, GFRP sheets are considered useless in the back of the column since the stress in this area is nearly zero.

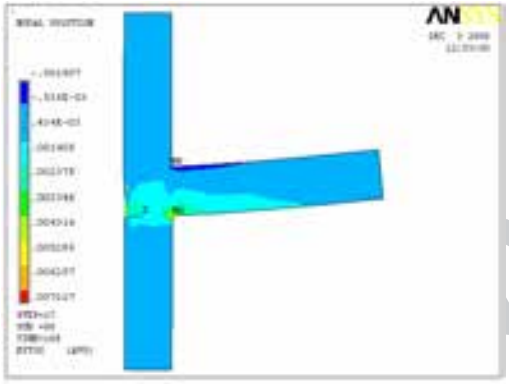

Fig. 26. Joint shear failure of specimen FM1-R extracted from numerical modeling

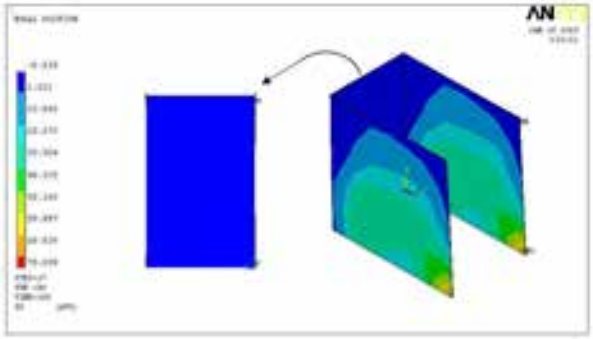

Fig. 27. Strain variation along the GFRP sheets of specimen FM1-R obtained from numerical modeling

d) Hysteretic curve of specimen FM1-R

Figure 28 shows the first hysteretic cycle for specimen FM1-R. As observed, this curve has three parts in the pull and push. The first part (OA) is a straight line, which describes the linear elastic behavior of reinforced concrete. Cracking causes a stiffness degrading and the direction to change toward point B. Then, in the BC region, the slope changes because yielding in the reinforcing bars has already begun. After unloading, in the next cycle, the response point moves toward the maximum displacement point in the preceding cycle (C).

e) Results of FE modeling for specimen FM2

The results obtained from FE modeling indicate that the maximum load capacity and maximum displacement of the joint are 199.6 kN and 27 mm, respectively. Furthermore, the cracking and yielding loads of the joint were found to be 29.1 kN and 170.7 kN, respectively; while their corresponding displacements respectively were 1.7 mm and 20.1 mm. As illustrated in Fig. 29, the maximum lateral displacement for this case in the push is 27 mm, while it is 22 mm in the pull. The maximum loads, in pull and push are 199.6 kN and 231.6 kN, respectively. The hysteretic curve has narrow loops and is slightly

thin in the middle of the curve. The failure mode for this case is a combination of flexural and shear modes (Fig. 30). This is because concrete strains are about 0.002 in the joint core and in the adjacent part of the beam, which is close to the concrete failure strain. In addition, Fig. 31 shows the reinforcing bar strain, confirming this failure mode as the strain in the reinforcing bars is greater than their yield strain (ε_y=0.002).

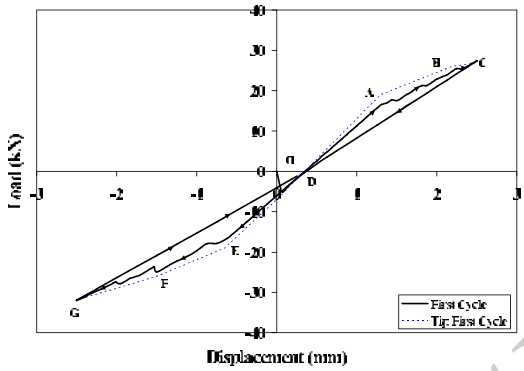

Fig. 28. Behavior of specimen MF1-R hysteretic curve

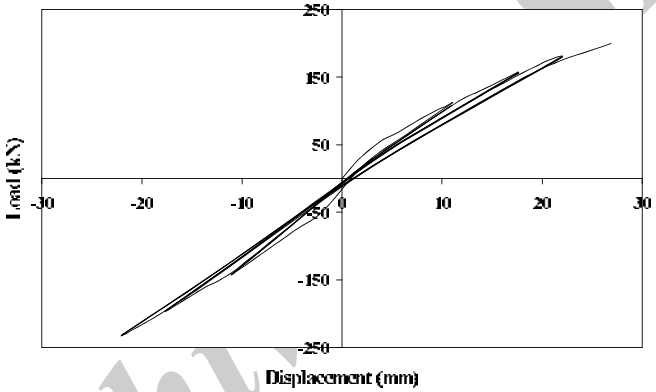

Fig. 29. Hysteretic curves for specimen FM2

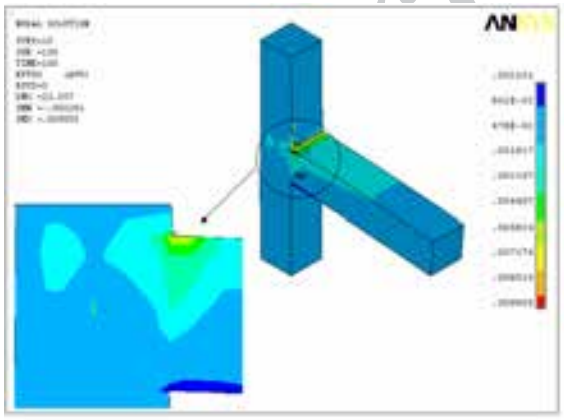

Fig. 30. Failure mechanism of FM2 obtained from numerical modeling

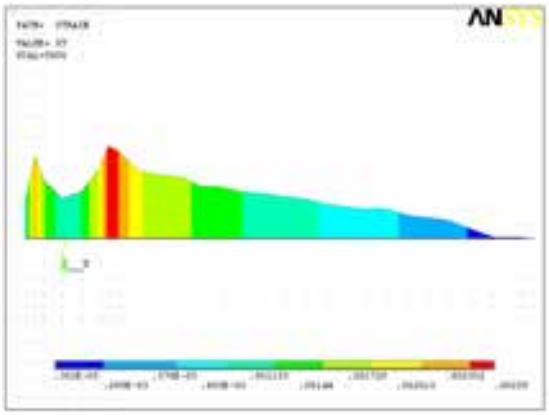

Fig. 31. Strain variation in the longitudinal reinforcement of FM2 obtained from numerical modeling

f) Results of FE modeling for specimen FM2-R

FM2-R specimen is subjected to the same loading regime as specimen FM2. For moving the plastic hinge from the face of the column toward the beam, CFRP sheets are used for strengthening. The 0.165 mm thick CFRP sheets had the tensile strength of 3900 MPa, modulus of elasticity of 260 GPa, and

ultimate elongation of 1.55%. The results indicate that the behavior of the joint is improved. Fig. 32 shows the final failure of the specimen in which the plastic hinge is formed beyond the cut–off point of the CFRP. In fact, CFRP reinforcement causes the plastic hinge to move from the face of the column toward the beam and the maximum strain in concrete to be more than 0.002. Reinforcing bar strain is less than the yield strain in the connection core (Fig. 33). Table 3 compares the failure, the cracking, and the load corresponding to the bars' yielding stress before and after strengthening. The decreased strain value indicates which CFRP plate can be useful for improving the joint behavior. As illustrated in Fig. 34, the maximum lateral displacement for this case in the push is 22.0 mm, while in the pull it is 26.1 mm. The maximum load capacities of the joint in the push and pull are 248.7 and 239.6 kN, respectively. FM2 & FM2-R hysteretic curves are compared in Fig. 35. The stiffness degradation decreases and load capacity increases by CFRP sheets in the strengthened specimen.

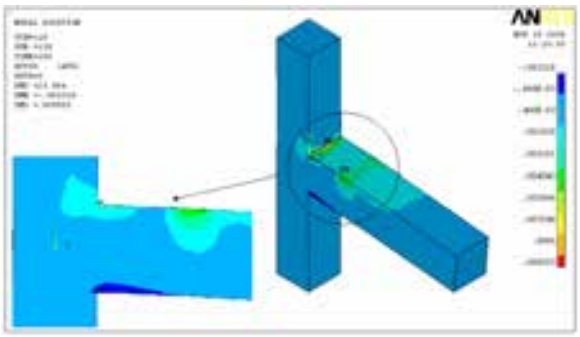

Fig. 32. Failure mechanism of FM2-R obtained from numerical modeling

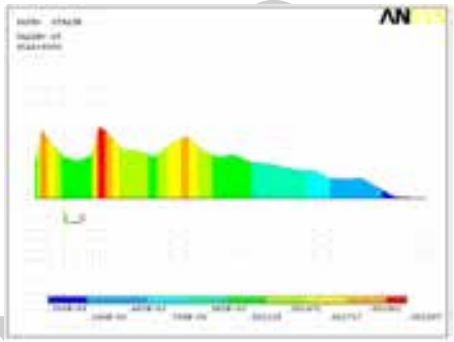

Fig. 33. Changing strain in the longitudinal reinforcement of FM2-R obtained from numerical modeling

Table 3. Comparison of specimens FM2 & FM2-R

Specimen	Cracking load (kN)	Yielding load (kN)	Failure load (kN)
FM2	27	170.7	199.58
FM2-R	42.31	206	239.57

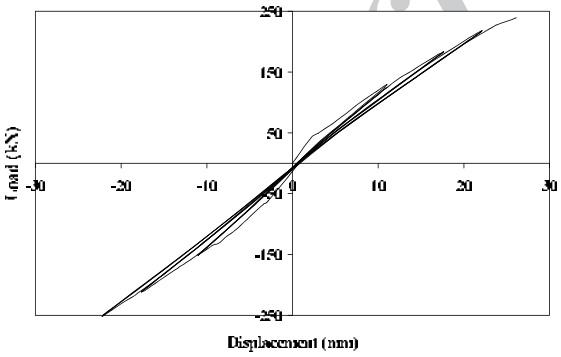

Fig. 34. Hysteretic curves for specimen FM2-R

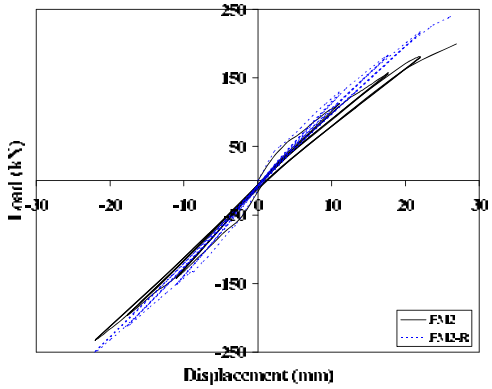

Fig. 35. Comparison of hysteretic curves obtained for FM2 & FM2-R specimen

g) Behavior of hysteretic curve of specimen MF2-R

The first hysteretic curve cycle of specimen FM2-R is shown in Fig. 36. OA is a straight line, which describes the linear elastic behavior of reinforced concrete. Then, because of cracking and stiffness, the degrading curve moves to B, which is the unloading point. After that, the displacement axis is cut by a straight line graph at point C, which starts the reverse loading. The explanation for this region is similar to

that for the previous one. After unloading, in the next cycle, the response point moves to the maximum displacement point in the preceding cycle (B).

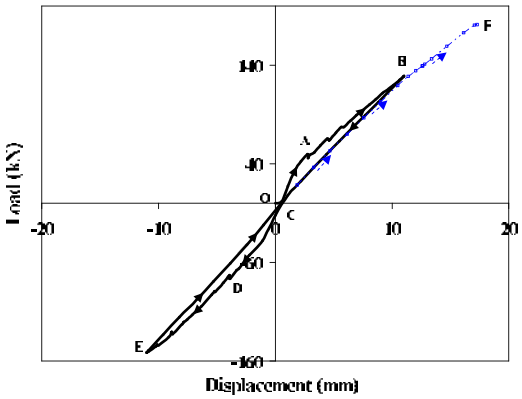

Fig. 36. Behavior of the hysteretic curve specimen of MF2-R

6. CONCLUSION

The capability of nonlinear finite element modeling in simulating the hysteretic behavior of RC exterior beam-column joints retrofitted with FRP sheets under cyclic loads was investigated in the current study. Three concrete beam-to-column joint specimens were selected and nonlinearly analyzed. The effects of bond slip between the concrete, reinforcing steel, and FRP sheets, and micro cracks occurring in the actual RC joints were excluded in the finite element models, contributing to higher stiffness of the finite element models. The general behavior of the finite element models represented by the hysteretic curve showed good agreement with the test data of the 1:2.5 scale joint [12] and full scale joint [16] tests. However, the finite element models showed slightly more stiffness than the test data. Other results of this study are summarized as follows:

1) Hysteretic curve in flexural joints has a wide loop, high strength, and more ductility and energy dissipation compared to that of the shear joints.
2) Cracking of concrete and its consequent stiffness degradation increase pinching and nonlinear behavior of hysteretic curve.
3) Strengthening FRP sheets in the connection zone moves the plastic hinge forward from the end of the beam to a reasonable distance, and decreases the maximum concrete strain in the joint region. Furthermore, they enhance the load carrying capacity, ductility and energy dissipation of the joint.
4) The modeling performed in this study on three specimens before and after being retrofitted, shows that finite element modeling can evaluate the cyclic performance of RC joints by adequate approximation. Therefore, the most effective retrofitting schemes under earthquake load may be easily recognized using the low cost finite element models.

REFERENCES

1. Paula, T., Park, R. & Priestley, M. J. N. (1978). Reinforced concrete beam- column joints under seismic actions. *JACI Proc*.
2. Otani, S. (1981). Hysterics models of reinforced concrete for earthquake response analysis. *Journal of Faculty of Engineering, University of Tokyo*, Vol. 7, p. 441.
3. Otani, S. & Cheung, V. W. T. (1981). Behavior of reinforced concrete columns under biaxial lateral load reversals, (II) test without axial load. *Publication 81-02, Department of Civil Engineering, University of Toronto.*

4. Ngo, D. & Scordelis, A. C. (1967). Finite element analysis of reinforced concrete beams. *Journal of the American Concrete Institute*, Vol. 64, No. 3, pp. 152-163.
5. Nilson, A. H. (1968). Nonlinear analysis of reinforced concrete by the finite element method. *Journal of the American Concrete Institute*, Vol. 65, No. 9, pp. 757-766.
6. Mahini, S. S., Ronagh, H. R. & Smith, S. T. (2004). CFRP-Retrofitted RC exterior beam-column connections under cyclic load. *Proc. of the Second International Conference on FRP Composites in Civil Engineering (CICE 2004),* Adelaide, Australia.
7. Mostofinejad, D. & Talaeitaba, S. B. (2006). Finite element modeling of RC connections strengthened with FRP laminates. *Iranian Journal of Science & Technology, Transaction B, Engineering*, Vol. 30, No. B1, pp. 21-30.
8. Parvin, A. & Wu, S. (2007). Ply angle effect on fiber composte wrapped reinforced concrete beam-column connections under combined axial cyclic loads. *Composite Structures, doi:10.1016/j.compstruct 2007.02.004.*
9. Xue, W., Li, L., Cheng, B. & Li, J. (2008). The reversed cyclic load tests of normal and pre-stressed concrete beams. *Journal of Engineering Structures*, Vol. 30, pp. 1014–1023.
10. Vasdravellis, G., Valente, M. & Castiglioni, C. A. (2008). Behavior of exterior partial-strength composite beam-to-column connections: Experimental study and numerical simulations. *Journal of Constructional Steel Research.*
11. Antonopoulos, Costas P. & Triantafillou, Thanasis C. (2003). Experimental investigation of FRP-strengthened RC beam-column joints. *Journal of Composites for Construction*, Vol. 7, No. 1, pp. 39-49.
12. Mahini, S. S., Ronagh, H. R. & Dux, P. F. (2004). Flexural repair of RC exterior beam-column joints using CFRP sheets. *Proc. of the Second International Conference on FRP Composites in Civil Engineering (CICE 2004), 8-10 December-Adelaide, Australia*, pp. 653-658.
13. Otani, S. (1980). Nonlinear dynamic analysis of reinforced concrete building structures. *Canadian Journal of Civil Engineering*, Vol. 7, No. 2, pp. 333-344.
14. ANSYS (2005). ANSYS Manual, ANSYS, INC., Canonsburg, PA 15317, USA.
15. AS 3600, 2001, Concrete Structures, Australia Standards, Homebush Bay, Australia.
16. Ghobarah, A. & Said, A. (2001). Seismic rehabilitation of beam-column joints using FRP laminates. *Journal of Earthquake Engineering*, Vol. 5, No. 1, pp. 113-129.
17. ACI Committee 318, (2005). Building code requirements for reinforced concrete (ACI 318-05) and commentary (ACI 318R-05). American Concrete Institute, Detroit, Michigan.